Department of Chemical Engineering
University of California, Santa Barbara

CH E 180A. Chemical Engineering Laboratory

Natural Convection Boundary Layer of Water Determined by Laser Doppler Velocimetry at Average Temperature Range from 33-55 °C

Sean Shen, Melody Spann, Yulun Wu
Group 8T

Experiment Conducted between May 7 and May 14, 2024
Report Submitted on May 21, 2024

1 Abstract

The study explores the velocity profile within the natural convective boundary layer adjacent to a heated vertical wall in a water tank. Utilizing Laser Doppler Velocimetry (LDV), fluid flow velocities driven by temperature gradients were non-invasively measured. Starch particles were introduced to trace fluid motion, and Doppler burst frequencies were recorded at wall temperatures of $36.0 \pm 0.1\,^{\circ}\mathrm{C}$, $50.0 \pm 0.1\,^{\circ}\mathrm{C}$, and $60.0 \pm 0.1\,^{\circ}\mathrm{C}$. Experiments were conducted to measure velocity at two vertical positions separated by 13 mm to determine vertical changes in the velocity profile. Each temperature condition was replicated twice and average values were calculated to minimize errors. Theoretical velocities profile for each different conditions are calculated and solved by PDE. Results indicate significant variations in velocity profiles due to temperature changes and vertical position changes, as velocity profiles become steeper and higher emphasizing the influence of natural convection and temperature gradients on boundary layer behavior. These findings enhance our understanding of heat transfer and fluid dynamics in natural convective systems, which are critical for optimizing industrial processes involving thermal management and design of heating systems.

2 Introduction

The density and viscosity of fluids largely depend on temperature, with fluids becoming less dense and viscous at higher temperatures. Thus, a temperature gradient results in a viscosity and density gradient, where buoyancy forces the hotter fluid to rise as the colder fluid moves to replace it, generating natural convection [**1**, **2**, **3**]. The frictional losses at the surfaces of pipes and walls develop fluid boundary layers, which must be accurately characterized to optimize the system. Since the boundary layer due to natural convection is very small, large measuring probes can significantly affect the measurements. Therefore, a non-invasive method such as Laser Doppler Velocimetry (LDV) is necessary to accurately characterize the local velocity profile without disturbance [**4**]. To better understand the effect of natural convection, the boundary layer within a water tank near a heated wall was measured and modeled [**5**]. The starch within the water tank acts as tracer particles as it moves along the direction of natural convection fluid flow, the movement of which is detected via LDV [**5**]. The natural convection of the water can be modeled by solving the continuity, Navier-Stokes, and heat equations, Equations 1-3 respectively.

$$\frac{\partial u}{\partial x} + \frac{\partial w}{\partial y} = 0 \tag{1}$$

$$u\frac{\partial u}{\partial x} + w\frac{\partial u}{\partial y} = v\frac{\partial^2 u}{\partial y^2} + g\gamma(T_w - T_\infty)\theta \tag{2}$$

$$u\frac{\partial \theta}{\partial x} + w\frac{\partial \theta}{\partial y} = \alpha\frac{\partial^2 \theta}{\partial y^2} \tag{3}$$

where u is the flow velocity along the heated wall in the x-direction in $\frac{m}{s}$, v is the flow velocity perpendicular to the heated wall in the y-direction in $\frac{m}{s}$, ν is the kinematic

viscosity of the fluid in $\frac{m^2}{s}$, g is the acceleration due to gravity in $\frac{m}{s^2}$, γ is the thermal expansion coefficient in $\frac{1}{^\circ C}$, T_w is the temperature of the heated wall in $^\circ C$, T_∞ is the temperature of the bulk fluid in $^\circ C$, α is the thermal diffusivity in $\frac{m^2}{s}$, and $\theta = \frac{T-T_\infty}{T_w-T_\infty}$ is a non-dimensional value used to simplify the boundary conditions of the system [**5**]. The partial differential equations (PDE) 1-3 can be further simplified to a system of ordinary differential equations (ODE) under the assumption that the system is at steady state, no-slip occurs at the wall, the bulk fluid is stagnant, and the boundary layers are thin

$$\xi''' + 3\xi\xi'' - 2(\xi')^2 + \theta = 0 \tag{4}$$

$$\theta'' + 3Pr\xi\theta' = 0 \tag{5}$$

where Pr is the Prandtl number, a non-dimensional ratio comparing the dissipation of momentum in a fluid to the dissipation of heat [**5**]. The ODE can be solved numerically through online programs to determine the theoretical velocity profile of the natural convection boundary layer using Equations 6 and 7 [**5**].

$$u(x,y) = 4\nu\sqrt{x}c^2\,\xi' \tag{6}$$

$$w(x,y) = \frac{vc}{x^{1/4}}(\eta\xi' - 3\xi) \tag{7}$$

The extent of the fluid boundary layer depends on the buoyant forces due to the thermal gradient and the viscous forces that resist flow, which is characterized by the dimensionless Grashof number

$$Gr = \frac{g\gamma(T_w - T_\infty)L^3}{\nu^2} \tag{8}$$

where L is the length of the heated surface [**6**]. Grashof numbers less than 4×10^8 describe the laminar flow of fluids, anything above it can be characterized as turbulent flow [**6**]. In LDV, the crossing of out-of-phase lasers causes a phenomenon known as Young's interference fringes [**5**]. These fringes arise from the constructive and destructive interference of the same laser source, with the fringe spacing calculated via Equation 9

$$\delta = \frac{\lambda}{2\sin(\beta/2)} \tag{9}$$

where δ is the distance between the interference fringes of the Doppler burst in nm, λ is the wavelength of the laser in nm, β is the angle between the crossed lasers in radians [**5**]. When a tracer particle moves through the fringe zone, it scatters the laser, generating a Doppler burst [**5**]. These bursts signify the modulation of light intensity due to scattering, and LDV is employed to experimentally ascertain the Doppler burst frequency at different points within the water tank, utilizing the Labview program [**5**]. The data is used to determine the vertical local flow velocity describing the natural convection boundary layer using Equation 10.

$$u = \omega \cdot \delta \tag{10}$$

3 Method

Laser Doppler Velocimetry (LDV) determines fluid flow velocity due to natural convection from temperature gradients [**5**]. The experimental setup, shown in Figure 1, depicts a water tank with starch particles placed against a heated wall with lasers crossing through the tank [**5**]. The setup measures the Doppler burst frequency associated with the starch particles to determine their velocity[**5**]. The temperature control system sets the desired wall temperature and displays real-time temperatures of the wall and bulk fluid. The Doppler burst frequencies are measured at wall temperatures of $36.0 \pm 0.1\,^{\circ}\mathrm{C}$, $50.0 \pm 0.1\,^{\circ}\mathrm{C}$, and $60.0 \pm 0.1\,^{\circ}\mathrm{C}$. Two replicates were taken at each temperature. The bulk fluid temperature steadily increases over time due to natural convection. Temperature gradient need to remain relatively constant by adding cold water.

Characterization of the local velocity profile requires measuring the horizontal and vertical positions along the vertical heated wall. Metal blocks are placed below the tank to increase the vertical height of the interference fringes to determine the change in the vertical position. At a given temperature, the Doppler burst frequency at two heights with a difference of 13 mm was measured. Thin natural convection boundary layer[**5**] is measured using micrometer. After aligning the laser parallel to the wall, measurements were taken in the horizontal y-direction, perpendicular to the heated wall. Air bubbles formed on the heated wall and action is needed to remove the bubble that may affect the accuracy for the measurements. After those disturbance to the system, measurements should be taken several minutes later to ensure the water tank reaches equilibrium.

The photo-detector detected Doppler bursts and relayed data to the program, which displayed laser intensity as a function of time, in real time, qualitatively shown in Figure 2. Lab personnel manually adjusted bounds to identify Doppler bursts, resulting in subjective data acquisition. The program used a fast Fourier transform (FFT) to display Doppler burst frequency within specified margins, showing peaks on a graph of weighting factors against Doppler burst frequency [**7**]. The frequency corresponding to the peaks were noted to calculate the vertical local velocity along the heated wall.

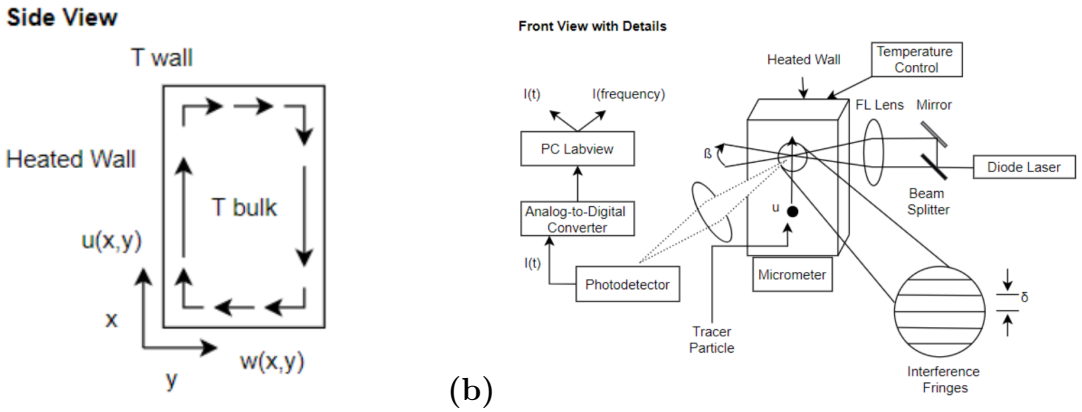

Figure 1: (a) Fluid flow and system geometry of the experimental setup where one vertical wall is heated. (b) LDV experimental setup to determine the vertical local velocity profile of fluid near a vertical heated wall. Micrometer is used to adjust the horizontal position of the laser and metal blocks, each measuring 13 mm height, are used to adjust the vertical position of the laser.

4 Results and Discussion

4.1 The Impact of Temperature and Temperature Gradients on the Momentum Boundary Layer

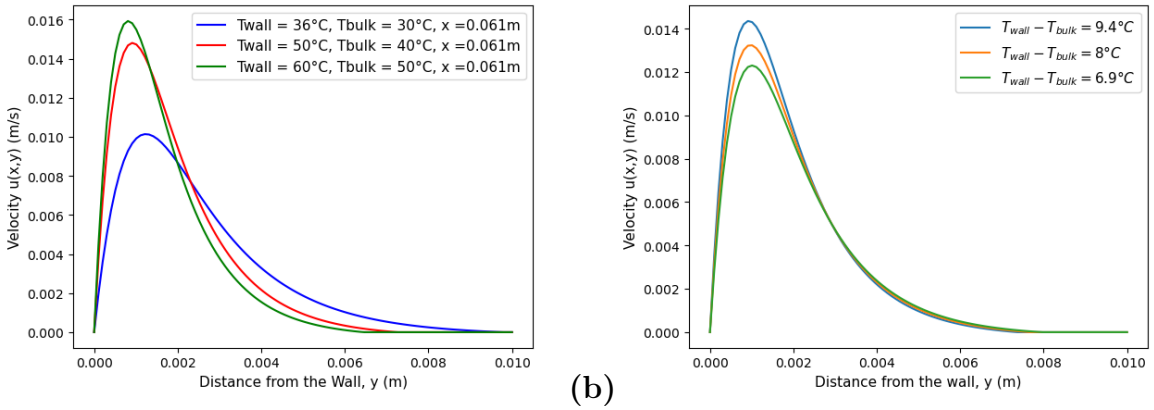

(a) (b)

Figure 2: Theoretical velocity profiles obtained by solving the PDE systems for trials with varying T_{wall} and T_{bulk}. (b) The plot illustrates the velocity profiles approximated using selected temperature gradients measured from a trial where $x = 0.061\,\text{m}$, $T_{\text{wall}} = 50°\text{C}$ and $T_{\text{bulk}} = 40°\text{C}$. The temperature gradient changes throughout the experiment due to constantly increasing T_{bulk}.

The maximum velocity for the theoretical boundary layer increases as temperature rises, and this maximum velocity is attained more quickly when T_{wall} and T_{bulk} become higher, as shown in Figure 2a. This trend corresponds with findings in other literature [**11**], and is primarily due to the decrease in fluid viscosity and the buoyancy effects resulting from thermal expansion. As the temperature of the fluid increases, viscosity decreases [**11**]. Simultaneously, as the fluid heats up, it expands, thus the fluid's density is reduced. This decrease in the fluid's density drives and enhances buoyancy forces, which cause the fluid to flow upward. The combination of decreasing density and increasing buoyancy forces leads to a steeper velocity gradient near the wall and higher maximum velocities within the boundary layer. The experimental Grashof number (Gr) calculated using Equation 8 varies from 5.5×10^7 to 1.5×10^8 during a temperature range of 33-55°C. Gr at 45 ± 0.05°C are about 0.8 times larger than the Gr at 33 ± 0.05°C (see Appendix B). The large Gr number at high temperatures indicates strong buoyancy forces associated with the fluid's small kinematic viscosity, thus corroborating the explanation above.

The impact of temperature gradients on the momentum boundary layer is also investigated. For example, the temperature gradient drops by 0.3-2.5°C during our experiment measuring $u(x, y)$ at $x = 0.061\,\text{m}$, $T_{\text{wall}} = 50°\text{C}$ and $T_{\text{bulk}} = 40°\text{C}$. This can be obtained from raw data in Appendix A. Taking this trial as an example, a high, an intermediate, and a low temperature gradient are selected and utilized to calculate their respective velocity profiles, as shown in Figure 2b. With a steeper temperature gradient, the fluid near the heated wall accelerates faster due to the stronger buoyancy forces. The fast-moving fluid driven by the strong buoyancy force near the wall results in a thinner momentum boundary layer because the velocity gradient near the wall becomes steeper.

4.2 Comparison of the Measured and Theoretical Velocity Profiles

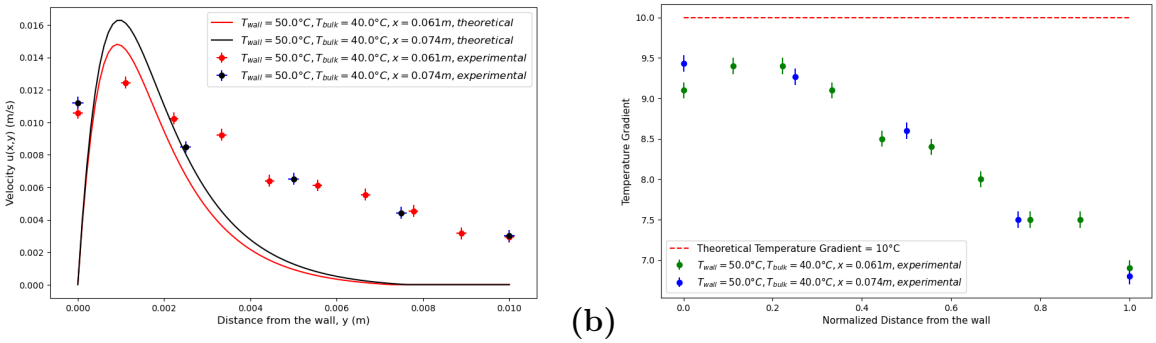

Figure 3: **(a)**Theoretical velocity profile alongside experimental values of point velocity $u(x, y)$ at $x = 0.061\,\text{m}$ and $x = 0.074\,\text{m}$, where $T_{\text{wall}} = 50°\text{C}$ and $T_{\text{bulk}} = 40°\text{C}$. Theoretical velocity profile is calculated using material properties of water at the average temperature of T_{wall} and T_{bulk}. **(b)** The plot displays the distribution of measured temperature gradient, while the temperature gradient used to calculate the theoretical velocity profile is constantly at 10°C

Local velocities $u(x, y)$ are calculated using measured data and Equation 10, and are overlaid with the theoretical velocity profiles with $x = 0.061\,\text{m}$ and $x = 0.074\,\text{m}$, whose $T_{\text{wall}} = 50°\text{C}$ and $T_{\text{bulk}} = 40°\text{C}$, as listed in Appendix C. According to the comparative plot, the measured point velocities agree with the overall quadratic shape of the predicted velocity profiles. However, as the normalized distance from the wall increases, the normalized measured velocities appear to be significantly higher than the velocities predicted by the boundary layer model.

This discrepancy might be due to the presence of measurement inaccuracies from the experiment setup. However, it is also important to note that the theoretical curves use material properties including kinematic viscosity, density, and thermal conductivity to approximate the velocity profiles. The approximation is accurate if the temperature gradient is constant throughout the experiment, but it cannot be achieved because T_{bulk} keeps increasing, as shown in Figure 3b. Therefore, based on the discussion in Section 3.1, because the boundary layer thickens as temperature decreases, the velocities measured further away from the wall appear to be larger than the velocities predicted, as shown in Figure 3a and Figure C7 for a closer snapshot approaching the bulk fluid region.

In addition, the x-position of $u(x, y)$ also affects the velocity profile of the boundary layer according to Figure 3a. Theoretically, the temperature gradient should be independent of the position [**10**]. However, as discussed, the temperature gradient cannot be controlled to remain constant during the experiment. Adding blocks under the water tank essentially causes the x-position at which point velocities are measured to be lower because the laser diode is mounted. A decrease in the x-position causes the temperature gradient to increase because the distance through which the flow travels toward the interference fringes is shortened. In other words, the bulk fluid has less time in contact with the heated wall, which results in a larger temperature gradient between T_{wall} and T_{bulk} at the point where measurement is taken. This larger temperature gradient results in the higher and thicker boundary layer profile that Figure 3a illustrates.

4.3 Application of boundary layers

Inspired by Professor Mclean from UCSB, who models the velocity and stress of deep-ocean currents using a natural boundary layer model[**11**], we can envision the ocean as a giant water tank. Convective boundary layers form within this tank due to temperature differences. By understanding the relationship between the boundary layer, temperature differences, and ocean depth, we can use theoretical boundary layer theory to model the velocity profile. This modeling helps identify positions within the ocean where currents have relatively high velocities. Consequently, people can efficiently harness these faster currents to build plants that utilize the ocean's mechanical power to generate electricity.

5 Conclusions

The natural convection boundary layer of water tested in this experiment. Local velocities u(x,y) were measured and calculated by Laser Doppler Velocimetry, and the thin boundary layer was successfully captured. Theoretical boundary layer under different temperatures was calculated to compare with the experimental data, which provides standard reference of the films' thickness and trend of change. If this experiment were repeated, it is recommended to use a more controllable setup, or measure the point velocities quickly within a shorter time frame because the temperature gradient changes as the bulk fluid is constantly heated. Moreover, rather than using averaged temperatures, measuring the temperature at the interference fringe directly could result in a more accurate theoretical estimation of the boundary layer. While this experiment explores and verifies water's boundary layer behaviors, it is also recommended to perform this experiment on other fluids to determine if empirical data supports the theoretical models.

References

[1] Schlichting, H. *Boundary Layer Theory*; McGraw-Hill: New York, 1987.

[2] Bird, R.B.; Stuart, W.E.; Lightfoot, E.N. *Transport Phenomena*; John Wiley & Sons: New York, 2006.

[3] Welty, R.E.; Wicks, J.R.; Wilson, C.E. *Fundamentals of Momentum, Heat, and Mass Transfer*; Wiley: New York, 1984.

[4] Ruck, B. Distortion of LDA fringe pattern by tracer particles. *Expt. Fluids* 1991, **10**, 349-354.

[5] Gordon, M. UC Santa Barbara, Department of Chemical Engineering; ChE 180A: *Chemical Engineering Laboratory Manual: Natural Convection Boundary Layers*; UC Santa Barbara: Santa Barbara, 2018.

[6] Smith, R.; Inomata, H.; Peters, C. Chapter 8 - Heat Transfer and Finite-Difference Methods. In *Supercritical Fluid Science and Technology*; Smith, R.; Inomata, H.; Peters, C., Eds.; Elsevier: 2013; Volume 4, pp 557–615. ISSN 2212-0505. ISBN 9780444522153. DOI: 10.1016/B978-0-444-52215-3.00008-8.

[7] Zonst, A.E. *Understanding the FFT*, 2nd ed.; Citrus Press: Titusville, FL, 1995.

[8] Deng, W.; Li, Z.; Ji, L.; Shang, L.; Liu, D.; Liu, X. Laser Doppler Velocimetry Test of Flow Characteristics in Draft Tube of Model Pump Turbine. *Processes* 2022, **10**, 1323. DOI: 10.3390/pr10071323.

[9] Ostrach, S. Natural Convection in Enclosures. In *Advances in Heat Transfer*; Hartnett, J. P., Irvine, T. F., Eds.; Elsevier: Volume 8, 1972; pp 161-227. DOI: 10.1016/S0065-2717(08)70039-X.

[10] Lee, J.; Hyun, M. T.; Kim, K. W. Natural convection in confined fluids with combined horizontal temperature and concentration gradients. *Int. J. Heat Mass Transfer* 1988, **31** (10), 1969-1977. DOI: 10.1016/0017-9310(88)90106-8.

[11] NIST Chemistry WebBook; National Institute of Standards and Technology: Gaithersburg, MD; Isobaric Properties for Water. Available online: `https://webbook.nist.gov/cgi/fluid.cgi?P=1&TLow=20&THigh=50&TInc=&Digits=5&ID=C7732185&Action=Load&Type=IsoBar&TUnit=C&PUnit=atm&DUnit=mol%2Fl&HUnit=kJ%2Fmol&WUnit=m%2Fs&VisUnit=uPa*s&STUnit=N%2Fm&RefState=DEF` (accessed May 21, 2024).

A Raw Data

1 block at average temperature 33°C+-0.05°C tiral 1			
T wall (±0.1°C)	T bulk (±0.1°C)	y (±0.0005 inch)	w(±1 Hz)
36.3	30.7	0	937.5
36.3	31.3	0.005	781.25
36.3	31.7	0.01	1210.94
36	29.8	0.015	1933.59
36.1	30.8	0.02	1425.78
36.1	31.1	0.025	1074.22
35.9	32.2	0.03	1054.69
36.1	32.5	0.035	1464.84
35.7	30	0.04	1250
35.7	30	0.045	2656.25
35.6	30.2	0.05	2127.66
35.9	30.6	0.055	1949.06
36	31.1	0.06	1486.49
36	31.3	0.065	1447.88
36	31.8	0.07	1196.91
36	31.1	0.075	2200.77

1 block at average temperature 33°C+-0.05°C trial 2			
T wall (±0.1°C)	T bulk (±0.1°C)	y (±0.0005 inch)	w(±1 Hz)
36	28.9	0	2832.03
35.7	29.1	0.01	2519.533
36	29.4	0.02	2031.25
36	29.9	0.03	1503.91
36.1	30	0.04	1015.62
36.1	30.6	0.05	761.79
35.9	28.2	0.06	1503.91
35.9	28.9	0.07	527.344

2 blocks at average temperature 33°C+-0.05°C trial 1			
T wall (±0.1°C)	T bulk (±0.1°C)	y (±0.0005 inch)	w(±1 Hz)
36	29.3	0	2299.46
35.9	29.3	0.01	2324.22
35.8	29.4	0.02	2128.91
35.9	29.6	0.03	2089.84
35.6	29.9	0.04	1718.75
35.9	30.3	0.05	1503.91
35.9	30.2	0.06	1035.16
35.9	29.9	0.07	2031.25
35.7	29.9	0.08	1582.03
36.1	30.1	0.09	1132.81

2 block at average temperature 33°C+-0.05°C trial 2			
T wall (±0.1°C	T bulk (±0.1°C)	y (±0.0005 inch)	w(±1 Hz)
36	29.3	0	1738.28
35.9	29.4	0.01	1640.62
36	29.5	0.02	1718.75
36.1	29.6	0.03	1289.06
36	29.9	0.04	1152.34
36	30.6	0.05	1933.59
35.8	28.6	0.06	976.562
35.7	28.7	0.07	839.894

1 block at average temperature 45°C+-0.05°C trial 1

T wall (±0.1°C)	T bulk (±0.1°C)	y (±0.0005 inch)	w(±1 Hz)
50.3	37.9	0.43	1988.212
50.7	38.1	0.435	1988.42
50.7	38.1	0.44	1891.89
50.8	38.7	0.445	1759.08
50.1	38.8	0.45	2485.66
50.1	39.1	0.455	2065.01
50.2	39	0.46	1930.5
50.3	39.1	0.465	975.143
50.5	39.2	0.47	1158.3

1 block at average temperature 45°C+-0.05°C trial 2

T wall (±0.1°C)	T bulk (±0.1°C)	y (±0.0005 inch)	w(±1 Hz)
50.1	41	0.395	2906.31
50.4	41	0.4	3416.99
50.4	41	0.405	2810.71
50.3	41.2	0.41	2533.08
50.3	41.8	0.415	1757.81
50.8	42.4	0.42	1679.69
50.6	42.6	0.425	1523.44
50.3	42.8	0.43	1247.64
50.8	43.3	0.435	868.726
50.4	43.5	0.44	810.811

1 block at average temperature 55°C+-0.05°C trial 1

T wall (±0.1°C)	T bulk (±0.1°C)	y (±0.0005 inch)	w(±1 Hz)
61.9	50	0.41	2953.67
61.8	50.1	0.415	2344.05
61.6	50.6	0.42	1969.41
61.6	51.1	0.425	1376.67
61.3	51.5	0.43	1185.47
61.2	52	0.435	1003.86
60.9	52.4	0.44	1023.17
61.1	52.5	0.445	772.201

1 block at average temperature 55°C+-0.05°C trial 2

T wall (±0.1°C)	T bulk (±0.1°C)	y (±0.0005 inch)	w(±1 Hz)
60.9	48.4	0.41	2084.13
60.9	48.9	0.415	2127.66
61.2	49.2	0.42	2263.06
60.9	49.4	0.425	1797.32
61.1	49.9	0.43	1395.94
61.2	50.3	0.435	1152.34
61.1	50.7	0.44	1054.69
61.1	51.1	0.445	878.906
61	51.2	0.45	683.594
61	51.7	0.455	664.062

1 block at average temperature 55°C+-0.05°C trial 2

T wall (±0.1°C)	T bulk (±0.1°C)	y (±0.0005 inch)	w(±1 Hz)
60.9	48.4	0.41	2084.13
60.9	48.9	0.415	2127.66
61.2	49.2	0.42	2263.06
60.9	49.4	0.425	1797.32
61.1	49.9	0.43	1395.94
61.2	50.3	0.435	1152.34
61.1	50.7	0.44	1054.69
61.1	51.1	0.445	878.906
61	51.2	0.45	683.594
61	51.7	0.455	664.062

2 block at average temperature 55°C+-0.05°C trial 1

T wall (±0.1°C)	T bulk (±0.1°C)	y (±0.0005 inch)	w(±1 Hz)
60.1	48.5	0.44	3808.59
59.8	48.9	0.445	3339.84
59.9	49.2	0.45	3320.31
60.2	49.6	0.455	3164.06
60.2	50.1	0.46	2642.77
59.9	50.3	0.465	2562.14
59.9	50.8	0.47	2332.7
60.1	51	0.475	2380.52
60.4	51.4	0.48	2091.42
60.3	52	0.485	2088.97

2 block at average temperature 55°C+-0.05°C trial 2

T wall (±0.1°C	T bulk (±0.1°C)	y (±0.0005 inch)	w(±1 Hz)
59.9	50.7	0.42	1891.89
60.1	50.9	0.42	1682.79
59.9	51.1	0.42	1624.76
60.4	51.4	0.43	1315.28
60	52	0.43	1289.06
60.2	52.3	0.43	1367.19
60.4	52.4	0.44	1093.75
60.4	52.4	0.44	1093.75
60.5	53	0.44	898.437
60.4	53.1	0.45	664.062
60.6	53.3	0.45	781.25
60.5	53.6	0.45	761.719
60.2	53.8	0.46	527.344
60.6	54	0.46	488.281
60.5	53.5	0.46	488.281

2 block at average temperature 45°C+-0.05°C trial 1			
T wall (±0.1°C)	T bulk (±0.1°C)	y (±0.0005 inch)	w(±1 Hz)
49.9	40.4	0.42	3655.71
49.9	40.7	0.42	2778.86
50.3	40.7	0.42	2798.43
50.3	40.8	0.43	2407.05
50.3	41	0.43	2250.49
50.1	41.1	0.43	2328.77
50.1	41.4	0.44	1996.09
50.3	41.5	0.44	1862.93
50.3	42	0.44	1505.79
50	42.4	0.45	1351.35
50.4	42.7	0.45	1139
50.2	43	0.45	1147.23
50.3	43.2	0.46	965.251
50.4	43.5	0.46	752.896
50.3	43.9	0.46	752.896

B Sample Calculations

B.1 Velocity calculation

Calculation of δ:

$$\delta = \frac{\lambda}{2 \cdot \sin(\beta/2)} = \frac{(635 \times 10^{-9})}{2 \cdot \sin(10 \times \pi/180)} = 3.64 \times 10^{-6}\,\mathrm{m} \tag{B.1}$$

Error calculation of δ:

$$\sqrt{\left(\frac{1}{2 \cdot \sin(10 \times \pi/180)}\right)^2 \cdot (1 \times 10^{-9})^2 + \left(-\frac{635 \times 10^{-9} \cdot \cos(10 \times \pi/180) \cdot (\pi/180)}{2 \cdot \sin^2(10 \times \pi/180)}\right)^2 \cdot (1)^2} = 4.27{\times}10^{-9}\,\mathrm{m} \tag{B.2}$$

Calculation for velocity (m/s):

$$v = \delta \cdot \omega = 3.64 \times 10^{-6} \times 937.5 = 3.41 \times 10^{-3}\,\mathrm{m/s} \tag{B.3}$$

Normalization of velocity:

$$\frac{v}{v_{\max}} = \frac{3.41 \times 10^{-3}}{9.68 \times 10^{-3}} = 0.35 \tag{B.4}$$

Error calculation for velocity:

$$\sqrt{(937.5)^2 \cdot (4.27 \times 10^{-9})^2 + (3.64 \times 10^{-6})^2 \cdot (100)^2} = 3.6 \times 10^{-4}\,\mathrm{m/s} \tag{B.5}$$

Error calculation for normalized velocity:

$$\sqrt{\left(\frac{1}{9.68 \times 10^{-3}}\right)^2 \cdot (3.6 \times 10^{-4})^2 + \left(\frac{-3.41 \times 10^{-3}}{(9.68 \times 10^{-3})^2}\right)^2 \cdot (3.6 \times 10^{-4})^2} = 0.04 \tag{B.6}$$

B.2 calculation of dimensionless number

Grashof number calculation:

$$Gr = \frac{g\beta(T_w - T_\infty)L^3}{\nu^2} = \frac{9.8 \times 3.282 \times 10^{-4} \times (36.3 - 31.3) \times (127.50 \times 10^{-3})^3}{(748.81 \times 10^{-9})^2} = 6.65{\times}10^{7} \tag{B.7}$$

Grashof number error calculation:

$$\sqrt{\left(\frac{g\beta(T_w - T_\infty)L^3}{\nu^2}\right)^2 \times 0.05^2 + \left(\frac{g\beta(-T_\infty)L^3}{\nu^2}\right)^2 \times 0.05^2} = 59445904.56 \tag{B.8}$$

Table B.1: average Grashof number calculation at different temperature

	Average temperature (±0.05 C)		
	33	45	55
Average Gr	5.92*10^7±2.8*10^7	9.96*10^7±3.8*10^7	1.30*10^8±4.7*10^7

Prandtl number calculation:

$$Pr = \frac{c_p \mu}{\kappa} = \frac{75.293 \times 748.81 \times 10^{-6} \times 1000}{18 \times 0.61884} = 5.06 \tag{B.9}$$

C Supplemental Graph

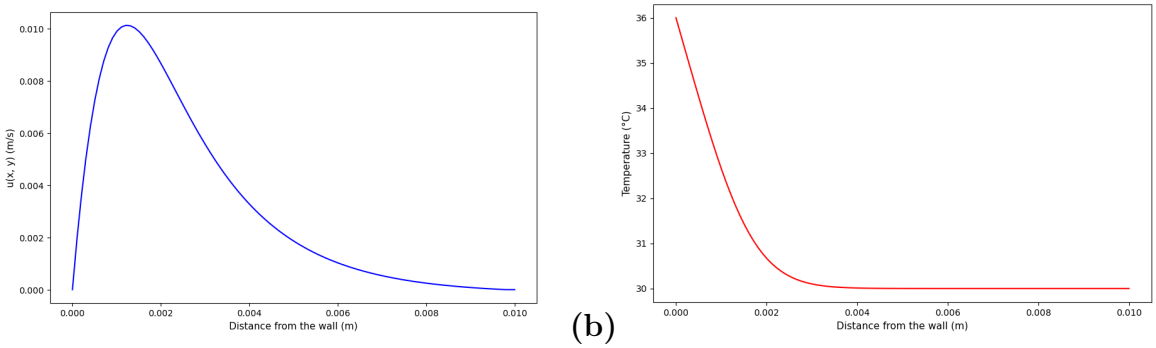

(a) (b)

Figure C1: Theoretical (a) velocity (b) temperature profile by solving PDE for natural convection boundary layer model for T_{wall} at 36 °C and T_{bulk} at 30 °C for x = 0.061m.

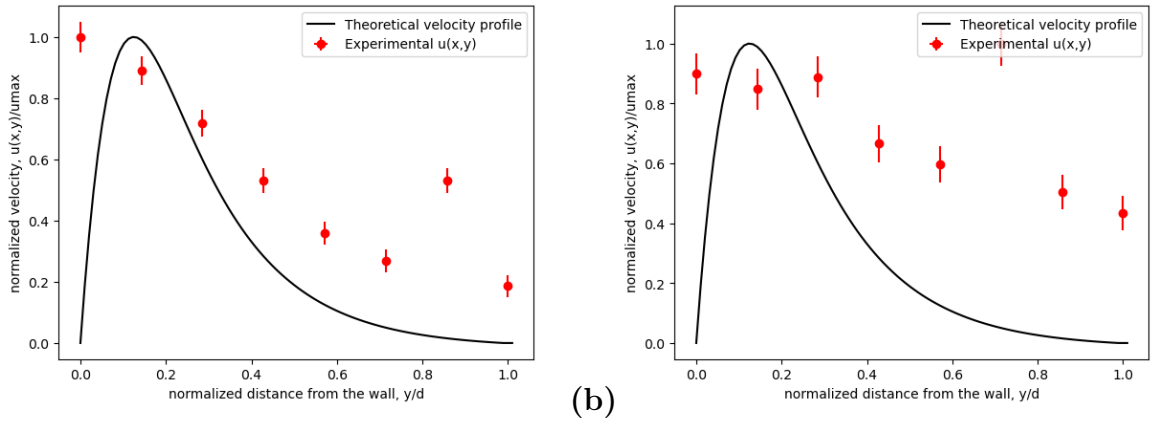

(a) (b)

Figure C2: Comparison of velocities calculated with the theoretical velocity profiles for T_{wall} at 36 °C and T_{bulk} at 30 °C for (a) x = 0.061m and (b) x = 0.074m. The horizontal bar represents the measuring uncertainty of the micrometer and the vertical error bar represents the propagated error for velocities calculated in appendix B.

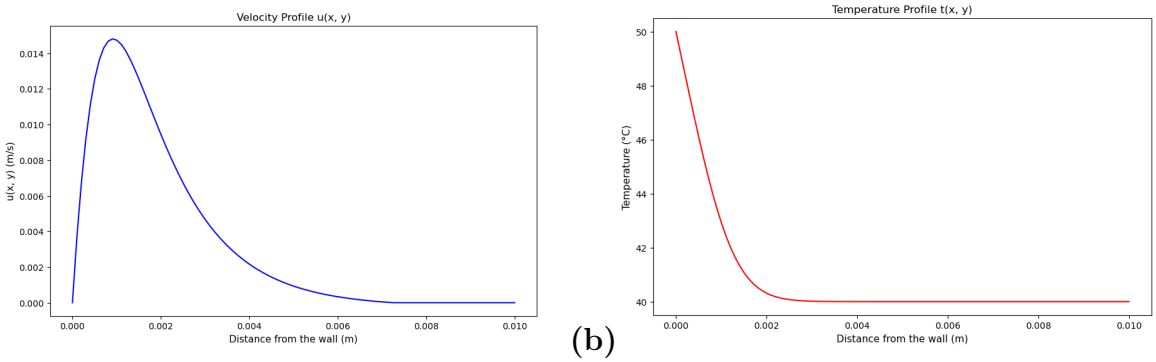

(a) (b)

Figure C3: Theoretical (a) velocity (b) temperature profile by solving PDE for natural convection boundary layer model for T_{wall} at 50 °C and T_{bulk} at 40 °C and for x = 0.061m.

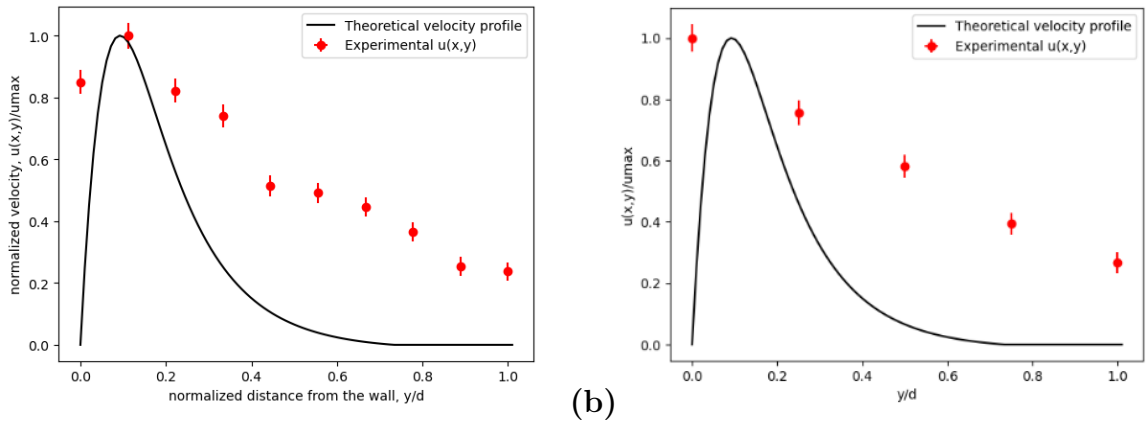

(a) (b)

Figure C4: Comparison of velocities calculated with the theoretical velocity profiles for T_{wall} at 50 °C and T_{bulk} at 40 °C for (a) x = 0.061m (b) x = 0.074m. The horizontal bar represents the measuring uncertainty of the micrometer and the vertical error bar represents the propagated error for velocities calculated in appendix B.

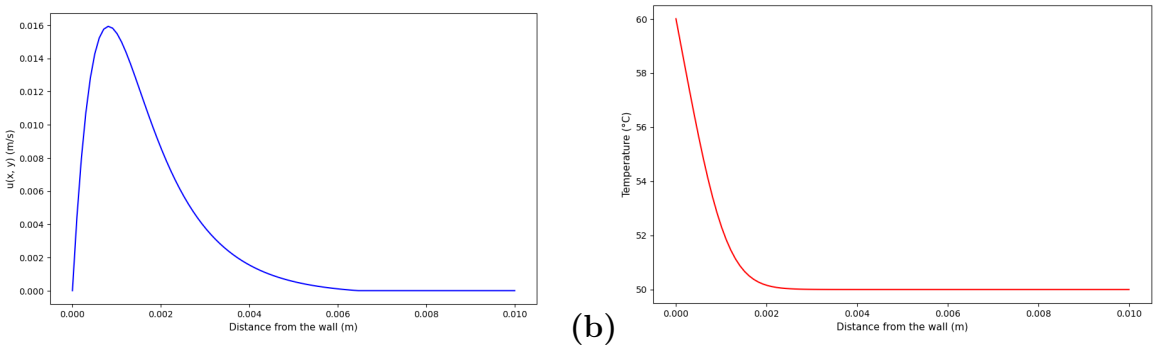

(a) (b)

Figure C5: Theoretical (a) velocity (b) temperature profile by solving PDE for natural convection boundary layer model forT_{wall} at 60 °C and T_{bulk} at 50 °C and for x = 0.061m.

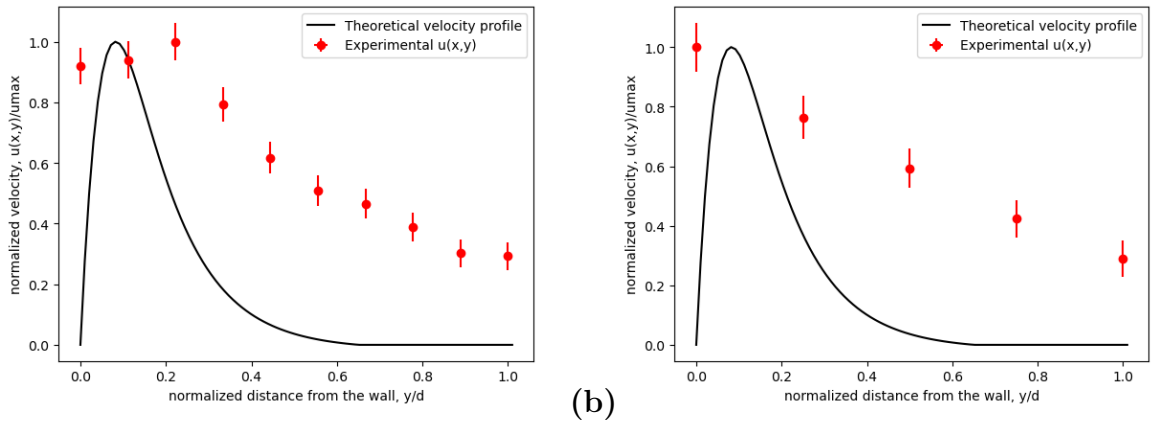

(a) (b)

Figure C6: Comparison of velocities calculated with the theoretical velocity profiles for T_{wall} at 60 °C and T_{bulk} at 50 °C for (a) x = 0.061m (b) x = 0.074m. The horizontal bar represents the measuring uncertainty of the micrometer and the vertical error bar represents the propagated error for velocities calculated in appendix B.

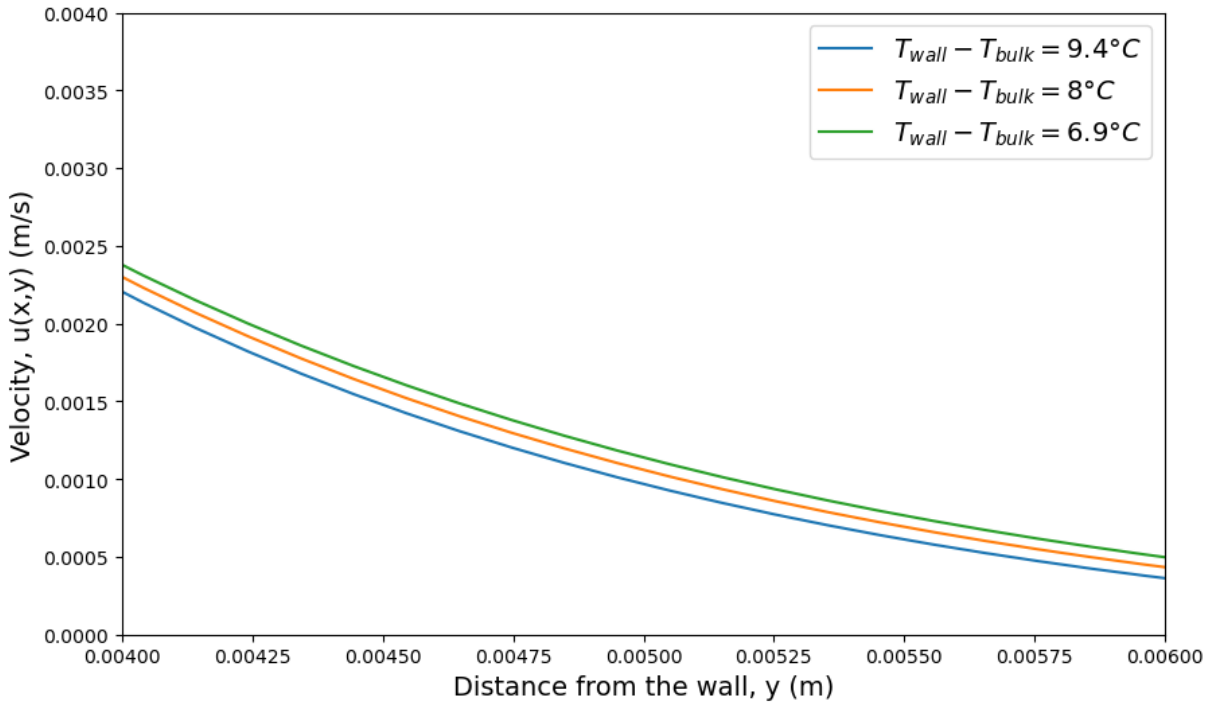

Figure C7: Closer snapshot of Figure 2b bulk fluid region's velocity profiles with changing temperature gradient

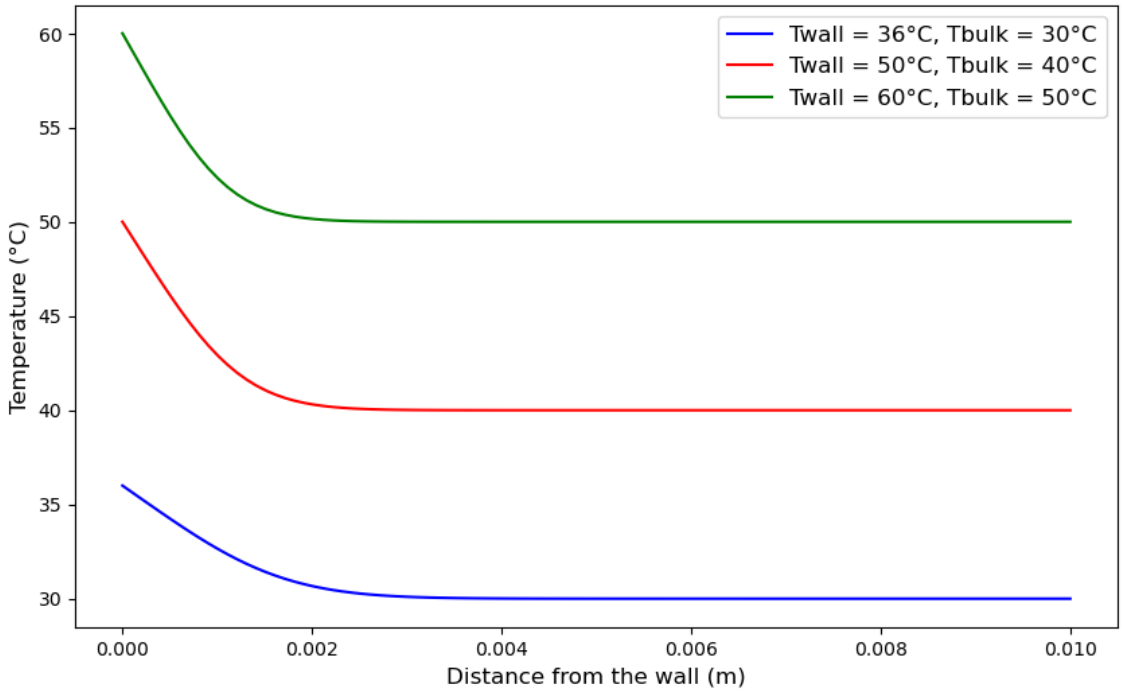

Figure C8: Theoretical temperature profiles calculated for the three different temperatures used toward the experiment

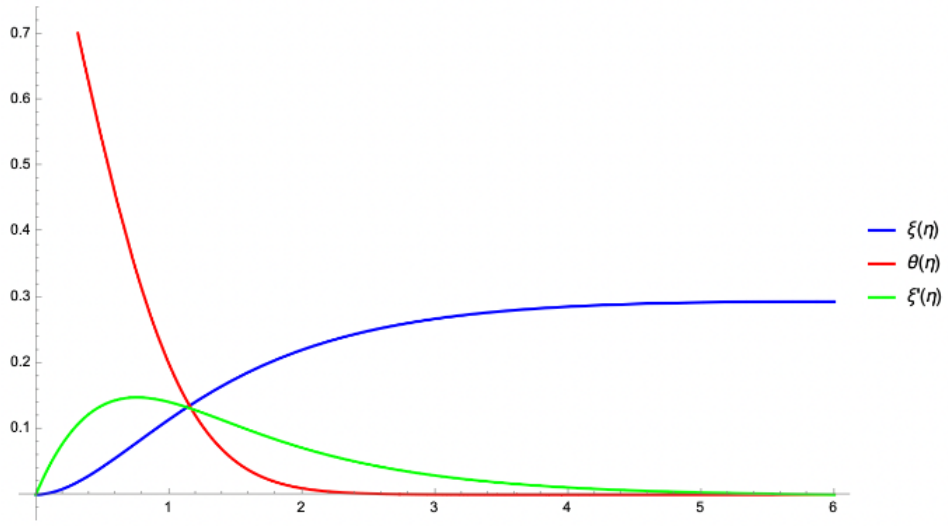

Figure C9: Plot of the non-dimensional velocity, temperature, and first derivative of the non-dimensional velocity versus non-dimensional distance away from the wall, characterized by transforming and solving the system of ODEs.

D program file

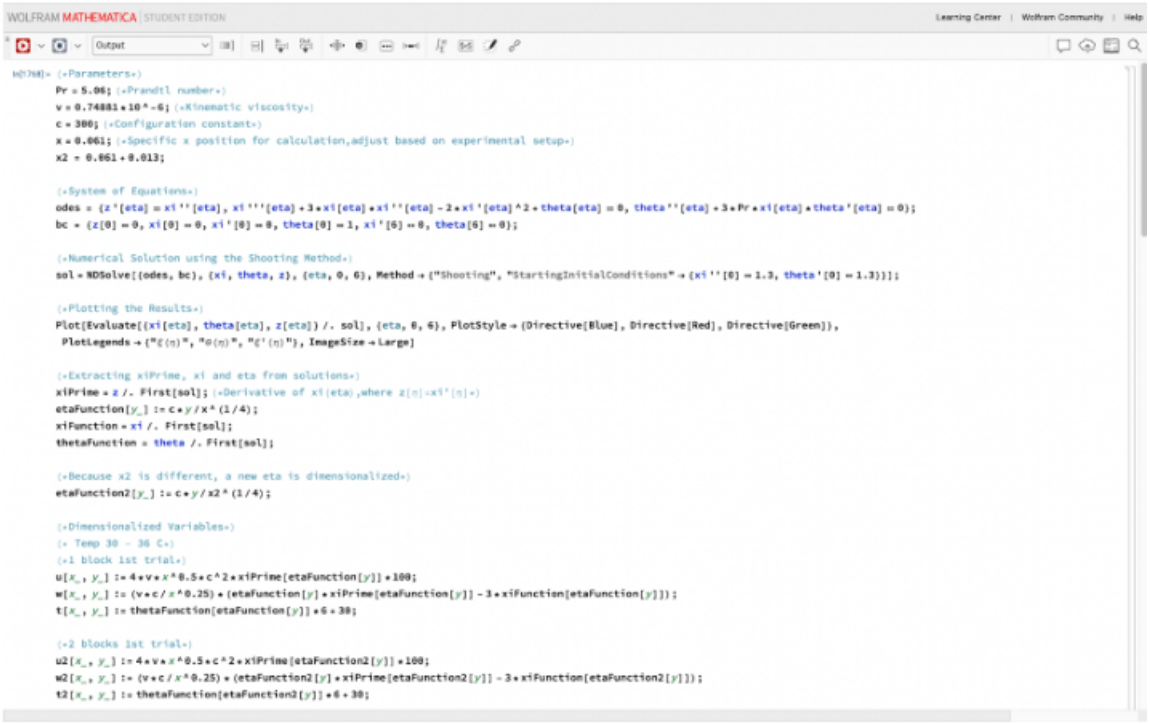

```
(*Parameters*)
Pr = 5.06; (*Prandtl number*)
v = 0.74881 * 10^-6; (*Kinematic viscosity*)
c = 300; (*Configuration constant*)
x = 0.061; (*Specific x position for calculation,adjust based on experimental setup*)
x2 = 0.061 + 0.013;

(*System of Equations*)
odes = {z'[eta] == xi''[eta], xi'''[eta] + 3 * xi[eta] * xi''[eta] - 2 * xi'[eta]^2 + theta[eta] == 0, theta''[eta] + 3 * Pr * xi[eta] * theta'[eta] == 0};
bc = {z[0] == 0, xi[0] == 0, xi'[0] == 0, theta[0] == 1, xi'[6] == 0, theta[6] == 0};

(*Numerical Solution using the Shooting Method*)
sol = NDSolve[{odes, bc}, {xi, theta, z}, {eta, 0, 6}, Method -> {"Shooting", "StartingInitialConditions" -> {xi''[0] == 1.3, theta'[0] == 1.3}}];

(*Plotting the Results*)
Plot[Evaluate[{xi[eta], theta[eta], z[eta]} /. sol], {eta, 0, 6}, PlotStyle -> {Directive[Blue], Directive[Red], Directive[Green]},
 PlotLegends -> {"ξ(η)", "Θ(η)", "ξ'(η)"}, ImageSize -> Large]

(*Extracting xiPrime, xi and eta from solutions*)
xiPrime = z /. First[sol]; (*Derivative of xi(eta),where z[η]=xi'[η]*)
etaFunction[y_] := c * y / x^(1/4);
xiFunction = xi /. First[sol];
thetaFunction = theta /. First[sol];

(*Because x2 is different, a new eta is dimensionalized*)
etaFunction2[y_] := c * y / x2^(1/4);

(*Dimensionalized Variables*)
(* Temp 30 - 36 C*)
(*1 block 1st trial*)
u[x_, y_] := 4 * v * x^0.5 * c^2 * xiPrime[etaFunction[y]] * 100;
w[x_, y_] := (v * c / x^0.25) * (etaFunction[y] * xiPrime[etaFunction[y]] - 3 * xiFunction[etaFunction[y]]);
t[x_, y_] := thetaFunction[etaFunction[y]] * 6 + 30;

(*2 blocks 1st trial*)
u2[x_, y_] := 4 * v * x^0.5 * c^2 * xiPrime[etaFunction2[y]] * 100;
w2[x_, y_] := (v * c / x^0.25) * (etaFunction2[y] * xiPrime[etaFunction2[y]] - 3 * xiFunction[etaFunction2[y]]);
t2[x_, y_] := thetaFunction[etaFunction2[y]] * 6 + 30;
```

Figure D10: Mathematica code utilized to transform the system of PDEs to ODEs in order to solve for the non-dimensional velocity and temperature of the in theory. u(x,y), w(x,y) and t(x,y) are corresponding local velocities and temperatures solved by dimensional analysis.

[14]:
```python
import numpy as np
import pandas as pd
import matplotlib.pyplot as plt

# Load the theoretical data from CSV files
xi_vals = pd.read_csv("C:\\Users\\Lun\\Downloads\\xiVals.csv", header=None, names=["eta", "xi"])
theta_vals = pd.read_csv("C:\\Users\\Lun\\Downloads\\thetaVals.csv", header=None, names=["eta", "theta"])
z_vals = pd.read_csv("C:\\Users\\Lun\\Downloads\\zVals.csv", header=None, names=["eta", "xi_prime"])
```

[17]:
```python
# Parameters
Cp = 75.357
mu = 503.62e-6
v = mu / 985.7
k = 0.64602
g = 9.81
B = 4.86e-4
Twall = 60
Tbulk = 50

Tdiff = Twall - Tbulk
Pr = Cp * mu / 18 * 985.7 / k
c = (g * B * Tdiff / 4 / v**2)**0.25
x = 0.061
x2 = 0.061 + 0.013

# Functions for eta
eta_function = lambda y: c * y / x**0.25
eta_function2 = lambda y: c * y / x2**0.25

# Define the velocity and temperature profiles
def u(x, y):
    eta = eta_function(y)
    xi_prime = np.interp(eta, z_vals["eta"], z_vals["xi_prime"])
    return 4 * v * x**0.5 * c**2 * xi_prime

def w(x, y):
    eta = eta_function(y)
    xi_prime = np.interp(eta, z_vals["eta"], z_vals["xi_prime"])
    xi_val = np.interp(eta, xi_vals["eta"], xi_vals["xi"])
    return (v * c / x**0.25) * (eta * xi_prime - 3 * xi_val)

def t(x, y):
    eta = eta_function(y)
    theta_val = np.interp(eta, theta_vals["eta"], theta_vals["theta"])
    return theta_val * Tdiff + Tbulk

def u2(x, y):
    eta = eta_function2(y)
    xi_prime = np.interp(eta, z_vals["eta"], z_vals["xi_prime"])
    return 4 * v * x**0.5 * c**2 * xi_prime
```

Figure D11: Python code used to extract the solved PDE solutions and evaluate relevant velocity and temperature profiles

```python
def w2(x, y):
    eta = eta_function2(y)
    xi_prime = np.interp(eta, z_vals["eta"], z_vals["xi_prime"])
    xi_val = np.interp(eta, xi_vals["eta"], xi_vals["xi"])
    return (v * c / x2**0.25) * (eta * xi_prime - 3 * xi_val)

def t2(x, y):
    eta = eta_function2(y)
    theta_val = np.interp(eta, theta_vals["eta"], theta_vals["theta"])
    return theta_val * Tdiff + Tbulk

# Plot the theoretical profiles
y_values = np.linspace(0, 0.01, 100)
u_values = [u(x, y) for y in y_values]
w_values = [w(x, y) for y in y_values]
t_values = [t(x, y) for y in y_values]

plt.figure(figsize=(10, 6))
plt.plot(y_values, u_values, label='u(x, y)', color='blue')
plt.xlabel('Distance from the wall (m)',fontsize=11)
plt.ylabel('u(x, y) (m/s)',fontsize=11)
plt.show()

plt.figure(figsize=(10, 6))
plt.plot(y_values, t_values, label='Temperature (°C)', color='red')
plt.xlabel('Distance from the wall (m)',fontsize=11)
plt.ylabel('Temperature (°C)',fontsize=11)
plt.show()
```

Figure D12: Python code used to plot u(x,y) vs. y-position under changing temperature gradients.